Check for updates

Ti₃C₂Tₓ-AuNP based paper substrates for label-free SERS detection of bacteria and multimodal antibacterials†

Boya Shi,[a] Li Jiang, ⓘ *[a] Ruikai Ma,[a] Weidan Zhao,[a] Yekai Zheng,[a] Wangwei Pan,[a] Mi Liu,[a] Shangzhong Jin[a] and Yan Zhou*[b]

Bacterial infections have become a serious global health problem due to the misuse of antibiotics which causes the emergence of antibiotic-resistant strains. Photothermal therapy (PTT) has been widely studied in recent years as a method to combat the development of bacterial resistance. However, PPT may cause damage to the human body due to excessive laser power. Therefore, it is important and urgent to develop a multifunctional platform that can sensitively detect bacteria and effectively inhibit or kill bacteria at low laser power. Herein, a novel multifunctional paper substrate of Ti₃C₂Tₓ-AuNP was successfully synthesized by a self-assembly and freeze-drying method for bacterial detection and photothermal sterilization at low laser power. The typical Gram-negative *Escherichia coli* (*E. coli*) and the Gram-positive Methicillin-resistant *Staphylococcus aureus* (MRSA) were used as models to perform label-free, rapid and sensitive detection of bacteria based on the surface-enhanced Raman spectroscopy (SERS) method with detection limits as low as 10^5 CFU mL^{-1} and 5×10^5 CFU mL^{-1}, respectively, demonstrating the paper substrate's ability to detect bacteria with sensitivity and accuracy. The paper substrate of Ti₃C₂Tₓ-AuNP exhibits significant antibacterial effects when irradiated with 808 nm light at a low laser power of only 300 mW cm^{-2} and a short irradiation time of 5 minutes, and the germicidal rates for *E. coli* and MRSA were 99.94% and 92.71%, respectively. At the same time, the paper substrate of Ti₃C₂Tₓ-AuNP also produces a variety of reactive oxygen species under 808 nm laser irradiation, resulting in photodynamic therapy (PDT). Accordingly, this paper substrate of Ti₃C₂Tₓ-AuNP can not only sensitively detect bacteria, but also has photothermal and photodynamic sterilization, providing a promising countermeasure for the clinical treatment of diseases caused by multidrug-resistant bacteria.

[a]College of Optical and Electronic Technology, China Jiliang University, Hangzhou 310018, P. R. China. E-mail: lijiang@cjlu.edu.cn

[b]Wenzhou Key Laboratory of Sanitary Microbiology, Key Laboratory of Laboratory Medicine, Ministry of Education, School of Laboratory Medicine and Life Sciences, Wenzhou Medical University, Wenzhou, Zhejiang, 325035, P. R. China. E-mail: zhouyan@wmu.edu.cn

† Electronic supplementary information (ESI) available. See DOI: https://doi.org/10.1039/d4ra03723e

1. Introduction

Ubiquitous pathogenic bacteria pose a serious danger to humans. The misuse of antibiotics leads to the emergence of antibiotic-resistant strains of bacteria, which further threatens human health.[1–3] Therefore, in order to prevent and treat bacterial disease infections, efficient detection of bacteria and antibacterial-resistant sterilization methods are particularly important. Common bacterial detection methods usually require cumbersome sample preparation and a long processing time, which hinders the rapid detection of pathogenic bacteria.[4,5] Surface enhancement of Raman scattering (SERS) has become a popular bacterial detection method in recent years due to its high sensitivity, ease of operation, rapidity and efficiency.[6] Xiang Lin's group studied a machine learning-driven 3D plasmonic cavity-in-cavity (CIC) SERS platform which was proposed for sensitive and quantitative detection of antibiotics.[7] Dan Wang *et al.*, developed to fabricate an ultra-thin layered flexible wearable SERS substrate, which consisted of biocompatible SF film as flexible support, ultrathin cavity AAO as template, and plasmonic AuNP.[8] Au or Ag nanomaterials are the most common SERS substrates because of their strong localized surface plasmon resonance effect (LSPR). As a new family of 2D materials, MXene has rapidly gained popularity due to its abundant surface electrons, high biocompatibility, and metal-like band structure, and has been widely used in the field of SERS.[9,10] In MXene/metal hybrids, their interfaces are very important to the interfacial electromagnetic enhancement (EM) and chemical enhancement (CT) enhancements, which greatly influence the final SERS performances.[11] Our group has reported many similar SERS substrates, among which Zizhen Yu *et al.*, have successfully synthesized a novel multifunctional MXene-Au nanocomposite by self-assembly method for rapid

detection and photothermal sterilization of bacteria.[12] Rongyang Liu reported a flexible SERS platform for the detection of dye molecules based on common laboratory filter paper modified with $Ti_3C_2T_x$ flakes.[13] However, the use of flexible MXene composites as SERS substrates for the detection of bacteria has not been addressed, which may limit the application in bacteria detection in some scenarios.[14]

In addition, MXene exhibits antibacterial properties by multiple routes. A. A. Shamsabadi *et al.* found that the good antibacterial properties of the smaller sized Ti_3C_2 nanosheets were attributed to the direct physical interaction between the sharp edges of the nanosheets and the bacterial membrane surface.[15] The bactericidal effect achieved through physical contact reduces the effect of bacterial resistance, but it usually takes a long time to achieve good bactericidal effect in this way. Photothermal therapy (PTT) has emerged as an effective antibacterial strategy. PTT relies on photothermal agents to convert near-infrared (NIR) light energy into localized physical heat to effectively kill bacteria. It has the advantages of high efficiency, good specificity, and minimally invasive to normal tissues. MXene has been reported to be widely used in photothermal therapy. As Yuwei Zheng *et al.*, reported, a hybrid hydrogel was constructed by incorporating Cip-Ti_3C_2 nanocomposites into the network structure of a Cip-loaded hydrogels to trap and kill bacteria.[16] In Chenhao Yu's work, it combined the photothermal effect of MXene with the photodynamic effect of indocyanine green (ICG), which had great anti-MRSA activity under NIR.[17] Despite the variety of materials, these photothermal agents typically require high laser power and are unable to provide useful therapeutic results without the use of high laser irradiation that can be harmful to the skin. For example, for the 808 nm laser, a widely used light source in photothermal research, an irradiation power density of ≥ 0.5 W cm^{-2} is used,[16-20] although the maximum value allowed to the skin at this wavelength is only 0.33 W cm^{-2} (ref. 21 and 22). In addition, MXene has been reported to possibly induce the generation of reactive oxygen species. As Gongyuan Liu *et al.* reported that ultrathin Ti_3C_2 MXene nanosheets have been synthesized by supplying additive Al^{3+} to avoid Al loss and employed as a photothermal/photodynamic agent for cancer therapy.[23] It is possible that the addition of photodynamic therapy has enhanced the sterilizing effect.

In our current work, we successfully synthesized $Ti_3C_2T_x$-AuNP nanocomposites by a self-assembly strategy and deposited it on cellulose paper by freeze-drying. Subsequently, *E. coli* and MRSA were used as models to verify the excellent performance of paper substrate of $Ti_3C_2T_x$-AuNP in label-free SERS detection, bacterial inhibition, photothermal and photodynamic therapy of bacteria. This study offers promising prospects for $Ti_3C_2T_x$ nanocomposites for rapid detection and low laser power sterilization in biomedical fields.

2. Experimental section

2.1. Materials and reagents

Titanium aluminum carbide powder (Ti_3AlC_2, 400 mesh) was purchased from FoShan XinXi Technology Co., Ltd (Guangzhou, China). Hydrochloric acid (HCl, 35–38%), lithium fluoride (LiF), (3-amino propyl)triethoxysilane (APTES, 98%), trisodium citrate ($C_6H_5Na_3O_7 \cdot 2H_2O$ 99.0%), 2.5% glutaraldehyde and ethanol (99.7%) were all purchased from Macklin (Shanghai, China). Chloroauric acid ($HAuCl_4$) was purchased from Adamas-beta Co., Ltd (Shanghai, China). NaCl (0.9%) were purchased from Yuanye Bio-Technology Co., Ltd (Shanghai, China). The bacterial strains *E. coli* and MRSA were purchased from the Sangon Biotech Co., Ltd (Shanghai China). Porcine serum was purchased from Stallion Biotechnology Co., Ltd (shanxi, China). Porcine skin was purchased from local market. The Lauria Broth (LB) agar was obtained from Sigma-Aldrich and stored at 4 °C. All reagents were analytical grade and were used without further purification.

2.2. Instruments

Scanning electron microscopy (SEM) images were obtained on ZEISS Sigma 300. X-ray diffraction (XRD) was measured on a powder diffractometer (D2 PHASER, Bruker) 2θ angle from 3° to 60° with Cu Kα radiation using 0.02° steps. UV-vis absorption spectra were collected by UV-vis spectrophotometer (TU-1901, PERSEE, Beijing). Raman spectra were collected by a Raman spectrometer with a 50 × lens (LabRAM HR Evolution, HORIBA), and all the detections were proceeded under a holographic grating of 600 g mm^{-1}. Excited lasers were 633 nm at room temperature. The SERS spectra were obtained with an accumulated time of 60 s. The NIR laser used for treatment was operated at 808 nm (Infrared Diode Laser system, Changchun CNI, China). Photothermal images and temperature data were collected by a PS400 High Performance Thermal Camera (Wuhan Guide Infrared Co., Ltd China).

2.3. Synthesis of paper substrate of $Ti_3C_2T_x$-AuNP

$Ti_3C_2T_x$ was synthesized according to the similar procedure described in our previous report.[12] Briefly, 1.6 g LiF was added to 20 mL of 9 M HCl and left under continuous stirring for 15 min. Then 1 g of Ti_3AlC_2 MAX powder was slowly added to the above solution and stirred at 35 °C for 24 h, the mixture was centrifuged for 10 min at 3500 rpm. The resulting acidic suspension was then washed using deionized (DI) water by centrifugation (5 min at 3500 rpm) until the pH of the supernatant reached about 6. Then, the $Ti_3C_2T_x$ precipitate was dispersed in 100 mL of DI water and sonicated for 30 min. After that, the mixture was centrifuged for 60 min to obtain the dark green supernatant, which was the resulting monolayer $Ti_3C_2T_x$ suspension. The prepared colloidal solution was stored at 4 °C for further use.

AuNP were synthesized by reducing $HAuCl_4$ with sodium citrate. 370 μL of $HAuCl_4$ solution (100 mM) was added to 100 mL of DI water and stirred until boiling. Subsequently, 1.3 mL of sodium citrate solution (1% w/v) was quickly added to the mixture and stirred for 30 min and cool to room temperature naturally. The final product was obtained from the above suspension and stored at 4 °C before the next use.

The $Ti_3C_2T_x$-AuNP was synthesized using self-assembly method. Firstly, 5 mL of ethanol was added to 10 mL of

$Ti_3C_2T_x$ solution and then 200 μL of APTES solution was added dropwise and stirred for 24 h. After the reaction, the suspension was washed 3 times with DI water for 10 min at 3500 rpm to remove the unreacted silane coupling agent. The final suspension was dispersed in 10 mL of DI. Next, 335 μL of APTES-$Ti_3C_2T_x$ dispersion and 40 mL of AuNP solution were mixed under stirring for 2 h at room temperature, and then sonicated for 30 min. After that, the mixture was centrifuged with 3500 rpm for 20 min. The supernatant was eliminated. Finally, 4 mL of DI was added to the residue to prepare $Ti_3C_2T_x$-AuNP solution.

The Whatman 3 mm cellulose chromatography filter paper was cut and soaked in the $Ti_3C_2T_x$-AuNP solution for 12 h. The soaked filter paper was put into −20 °C to pre-freeze for more than 2 hours. Then freeze-dry in a vacuum freeze-dryer. Finally, paper substrate of $Ti_3C_2T_x$-AuNP was obtained.

2.4. SERS measurement

E. coli and MRSA were cultured in LB until the initial concentration of bacterial strains was approximately 10^{10} colony forming units CFU mL^{-1}. Next, bacteria were centrifuged at 10 000 rpm for 2 min and sediment obtained were washed three times with NaCl solution (0.9%) to remove residual macromolecules and other growth medium constituents. Following that, bacterial suspension was diluted with NaCl (0.9%) solution, and then stored at 4 °C for future use. The paper substrate of $Ti_3C_2T_x$-AuNP was immersed in the different concentration bacteria suspension for 12 h and then dried in air. Then, the specimen was measured using a Raman microscope. Porcine skin was cut and dripped with bacteria, and the paper substrate of $Ti_3C_2T_x$-AuNP was attached to the porcine skin containing bacteria. Porcine serum was mixed with the bacteria and left to be tested. Subsequently, the paper substrates of $Ti_3C_2T_x$-AuNP were rinsed with DI and dried for further testing.

2.5. Antibacterial activity assessment

The antibacterial properties of paper substrate of $Ti_3C_2T_x$-AuNP were evaluated using *E. coli* and MRSA as the model Gram-negative and Gram-positive bacteria, respectively. The antibacterial effect of the paper substrate of $Ti_3C_2T_x$-AuNP was evaluated by the colony counting method. Firstly, 5 μL of bacteria (10^{10} CFU mL^{-1}) suspension was dropped on cellulose paper soaked in 200–800 μg mL^{-1} $Ti_3C_2T_x$-AuNP, $Ti_3C_2T_x$ and AuNP, and incubated on the shaker (37 °C, 200 rpm) for 5 hours. This allows bacteria to fully contact with the material and fall off the cellulose paper. A control group was prepared by dropping 5 μL of bacteria (10^{10} CFU mL^{-1}) suspension on cellulose paper soaked in NaCl solution (0.9%). Then, aliquots of the samples were withdrawn and CFU were counted by plating 100 μL of 10-fold serial dilutions onto LB agar plates. All plates were cultured in the dark at 37 °C until bacterial colonies became visible and countable. The survival rate of bacterial cells is calculated according to the following equation: bacterial survival rate = $N_m/N_c \times 100\%$, where N_c is bacterial colonies of the control sample and N_m is colonies for cells treated with paper substrate of $Ti_3C_2T_x$-AuNP.

2.6. Photothermal antibacterial activity assessment

Firstly, 5 μL of bacteria (10^{10} CFU mL^{-1}) suspension was dropped on cellulose paper soaked in 200–800 μg mL^{-1} $Ti_3C_2T_x$-AuNP nanocomposite, $Ti_3C_2T_x$ and AuNP. A control group was prepared by dropping 5 μL of bacteria (10^{10} CFU mL^{-1}) suspension on cellulose paper soaked in NaCl solution (0.9%). Then, the paper was immediately illuminated with NIR laser (808 nm, 5 min, 10 cm distance, 300 mW cm^{-2}). Photothermal images and temperature data were collected by a PS400 High performance thermal camera. After the irradiation is completed, the paper incubated on the shaker (37 °C, 200 rpm) for 5 hours. Finally, aliquots of the samples were withdrawn and CFU were counted as described previously.

2.7. Determination of reactive oxygen species

1,2-Phenylenediamine tablet (OPD), Nitrotetrazolium Blue chloride (NBT) and 1,3-Diphenylisobenzofuran (DPBF) were used to detect hydroxyl radical ($^\cdot$OH), superoxide anion radical ($O_2^{\cdot-}$) and singlet oxygen $^1O_2$. Briefly, the paper substrate of $Ti_3C_2T_x$-AuNP was placed into 2 mm quartz cuvettes containing 600 μL of probe solution. UV-vis absorption measurements were made with TU-1901 in quartz cuvettes after 808 nm laser irradiation every five minutes.

3. Results and discussion

3.1. Characterization of paper substrate of $Ti_3C_2T_x$-AuNP

The process for the preparation of paper substrate of $Ti_3C_2T_x$-AuNP is shown in Fig. 1a and b. $Ti_3C_2T_x$-AuNP is formed from $Ti_3C_2T_x$ and AuNP by self-assembly and then uniformly deposited on the surface of cellulose filter paper by freeze-drying.

To enlarge the surface area and delaminate MAX into several layers of nanosheets, the $Ti_3C_2T_x$ is prepared from Ti_3AlC_2 powders. As we reported previously, $Ti_3C_2T_x$ was prepared by Ti_3AlC_2 etched the intermediate Al layer. Fig. 2a shows the XRD patterns of Ti_3AlC_2 and $Ti_3C_2T_x$. It shows that after mixed etchant treatment, the peak at $2\theta \approx 39°$ [corresponding to the (104) plane] disappears, which proves Al atoms have been removed from Ti_3AlC_2. In addition, compared with pristine Ti_3AlC_2, the (002) diffraction peak of $Ti_3C_2T_x$ nanosheets is broadened and shifted to a lower angle, which confirms that the interlayer spacing of $Ti_3C_2T_x$ nanosheets has increased.[24] As shown in the SEM image (Fig. 2d), the $Ti_3C_2T_x$ nanosheets display a large surface area and sharp edges after etching. Fig. 2b shows the Raman of Ti_3AlC_2 and $Ti_3C_2T_x$. Comparison of Raman spectra of Ti_3AlC_2 and etched $Ti_3C_2T_x$. The peaks at 123 cm^{-1} and 202 cm^{-1} corresponds to a group vibration of carbon, two titanium layers, and surface groups. The peaks at 377 cm^{-1} and 580 cm^{-1} corresponds to surface group vibration. And the peak at 719 cm^{-1} corresponds to the vibration of the carbon. A_{1g} (Ti, C) at 182 cm^{-1} and 199 cm^{-1} vibrations of MAX phase shifted to 202 cm^{-1} because of etching and MXene formation. The disappearance of A_{1g} (Ti, Al) at 270 cm^{-1} is further evidence that the Al layer has been etched.[25]

As reported, AuNP were synthesized by reducing HAuCl$_4$ with sodium citrate.[26] In order to assemble AuNP on the surface of
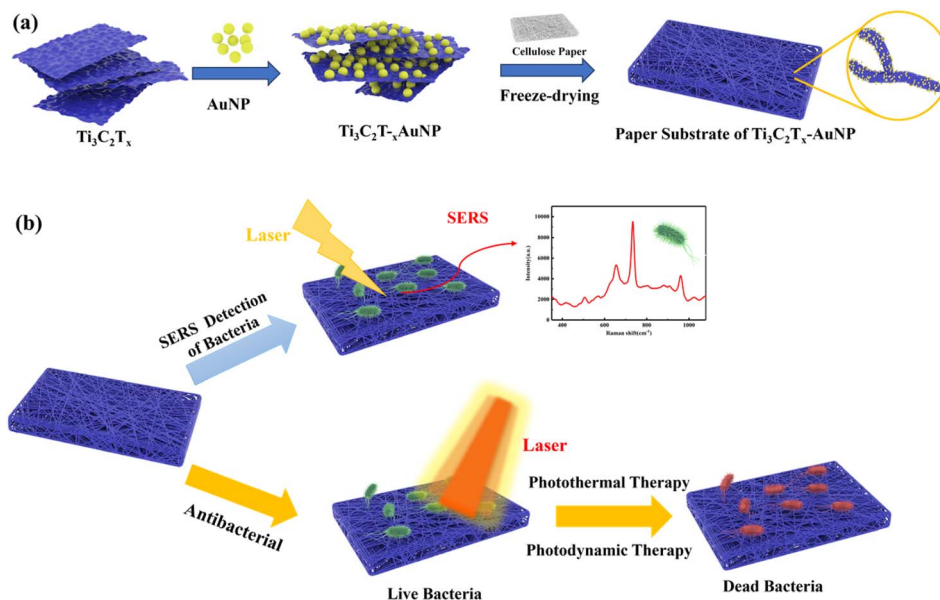
Fig. 1 Schematic illustration of (a) the preparation of paper substrate of $Ti_3C_2T_x$-AuNP. (b) SERS detection of bacteria and multi-therapeutic antibacterial by paper substrate of $Ti_3C_2T_x$-AuNP exposed to NIR laser.

$Ti_3C_2T_x$ nanosheets, the surface of $Ti_3C_2T_x$ is modified with amino groups and connected through dehydration condensation of APTES. The morphology and microstructure of AuNP and $Ti_3C_2T_x$-AuNP are characterized through SEM images (Fig. 2e and f). The results show that the diameter of AuNP is about 45 nm and they are evenly and densely distributed on the
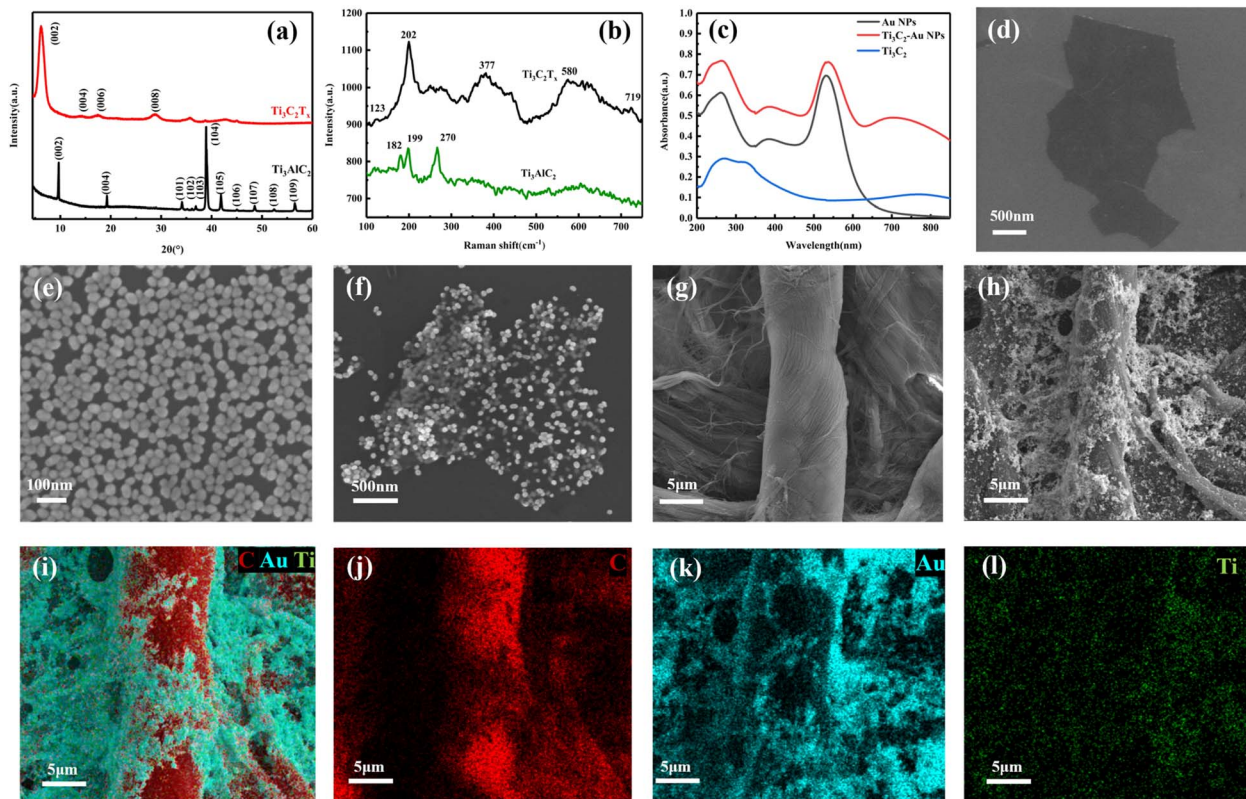

Fig. 2 (a) XRD patterns of $Ti_3C_2T_x$ and Ti_3AlC_2. (b) SERS spectra of $Ti_3C_2T_x$ and Ti_3AlC_2. (c) UV-vis spectra of AuNP, Ti_3C_2 and Ti_3C_2-AuNP suspensions. SEM of: (d) monolayer $Ti_3C_2T_x$ nanosheet, (e) Au nanoparticles, (f) $Ti_3C_2T_x$-AuNP nanocomposite, (g) paper substrate, (h) paper substrate of $Ti_3C_2T_x$-AuNP. Elemental mapping image of C (j), Au (k), Ti (l), and their overlay distribution (i).

$Ti_3C_2T_x$ nanosheets. Fig. 2c shows the UV-vis spectroscopy results for AuNP, $Ti_3C_2T_x$ and $Ti_3C_2T_x$-AuNP suspensions. The absorbance of $Ti_3C_2T_x$-AuNP at 600–850 nm was significantly higher than AuNP. The $Ti_3C_2T_x$-AuNP composites showed a red-shift of the absorption peak at 532 nm compared to AuNP, which proved the change of the local refractive index in the vicinity of the AuNP and the broadening of the absorption peak. This indicates that $Ti_3C_2T_x$-AuNP nanocomposites were successfully prepared.[12] Fig. 2g and h shows the comparison of cellulose paper before and after loaded $Ti_3C_2T_x$-AuNP. As shown in the SEM image (Fig. 2h), $Ti_3C_2T_x$-AuNP are uniformly and densely distributed on the fibers of cellulose paper. In addition, elemental map analysis (Fig. 2i–l) shows that Ti, C, and Au elements are evenly distributed on the fibers of cellulose paper. Therefore, these results indicate that $Ti_3C_2T_x$-AuNP are successfully adsorbed on the cellulose paper surface.

3.2. SERS properties of paper substrate of $Ti_3C_2T_x$-AuNP

MXene has been reported to have plasmon resonance effects in the visible and near-infrared range. Combined with the rich surface functional group of MXene, it can effectively combine more metal nanostructures and analyte molecules, and is promising to become an excellent SERS substrate.[9,27,28] It is well known that infections by pathogenic bacteria cause serious damage to human health and social security. Among them, E. coli and MRSA, as two common and dangerous pathogens, are urgently needed for immediate detection in the pre-infection stage.[29–31] In addition, compared to the common silicon-based SERS substrate, the flexible paper-based SERS substrate has the advantages of being more portable, fitting more closely to the surface to be inspected, and being able to be split for inspection. A cellulose paper with weak background signal was chosen as the paper substrate (Fig. S7†). In the paper substrate of $Ti_3C_2T_x$-AuNP, $Ti_3C_2T_x$-AuNP is uniformly and tightly deposited on the fibers of the filter paper, which allows the detected object to better contact with $Ti_3C_2T_x$-AuNP. Paper substrate of $Ti_3C_2T_x$-AuNP may be endowed with more unparalleled SERS performance than silicon-based SERS substrates. To demonstrate this, E. coli and MRSA were tested using the paper-base and silicon-based, respectively. Fig. 3a shows the SERS spectra of paper-based and silica-based at 5×10^6 and 10^6 CFU mL^{-1} bacterial concentrations, which reveals characteristic peaks at 657 cm^{-1}, 735 cm^{-1} and 962 cm^{-1} assigned to G, COO$^-$ str (Tyr), Glycosidic ring mode of A and polyadenine in FAD and NAD and C=C def, C–N str, respectively.[32] As shown in Fig. 3a, when the concentration of E. coli is 5×10^6, the silicon-based only has a weakly E. coli characteristic peak at 657 cm^{-1}. And when the concentration decreased to 10^6, the silicon-based showed almost no characteristic peak. Meanwhile, the paper-based exhibited strong characteristic peaks at both concentrations. There is no doubt that the paper-based exhibited better SERS performance. Besides, Fig. 3c shows the SERS spectra of E. coli in concentrations varying from 10^8 CFU mL^{-1} to 10^5 CFU mL^{-1}. According to previous research, the LOD of the assay is estimated based on the signal-to-noise ratio of detected spectral peaks greater than three, where signal is the peak height of the

analyte molecule at the lowest concentration and noise is the peak background. The results showed that the detection limit was as low as 10^5 CFU mL^{-1}, which proved that the paper substrate of $Ti_3C_2T_x$-AuNP had good SERS performance. Similarly, MRSA was used to assay the SERS performance of paper substrate of $Ti_3C_2T_x$-AuNP. A similar situation occurred with the detection of MRSA. As shown in Fig. 3b, the paper-based had better SERS performance than the silicone-based for MRSA. Fig. 3d shows the SERS spectra of MRSA in concentrations varying from 10^8 CFU mL^{-1} to 5×10^5 CFU mL^{-1} and reveals characteristic peaks at 660 cm^{-1}, 734 cm^{-1} and 960 cm^{-1} assigned to $\delta(COO^-)$ guanine, tyrosine and aromatic rings, respectively.[33] The results showed that the detection limit was as low as 5×10^5 CFU mL^{-1} for MRSA. Therefore, the above experimental results demonstrate that the present paper substrate of $Ti_3C_2T_x$-AuNP biosensor exhibits excellent SERS performance.

Considering the practical application scenarios, the homogeneity and stability of biosensors are crucial to maintain their sensing performance. An ideal SERS biosensor should have good reproducibility and homogeneity. To evaluate the homogeneity of paper substrate of $Ti_3C_2T_x$-AuNP, Raman measurements were performed at 15 randomly selected locations on the substrate. The SERS spectra of the characteristic peaks of E. coli at different points were highly consistent (Fig. 3e). In addition, the statistical analysis of the intensities of their characteristic peaks showed that the relative standard deviation (RSD) of the Raman characteristic peak at 735 cm^{-1} was 12.7% (Fig. 3e), which indicated that the paper substrate of $Ti_3C_2T_x$-AuNP was homogeneous over a large area. In the stability test, the SERS intensity of E. coli at 735 cm^{-1} was essentially unchanged within one month compared with the newly prepared substrate (Fig. 3f).

The analysis of actual samples is an integral part of the SERS detection. In our work, porcine skin and porcine serum were selected as actual samples. For the analysis of porcine skin samples, as shown in Fig. S8,† the characteristic peak intensity of tyrosine of MRSA at 734 cm^{-1} decreased with decrease MRSA concentration, and the detection limit was as low as 5×10^5 CFU mL^{-1}. In the detection of porcine serum (Fig. S9†), although the peak was broadened due to the interference of serum, the characteristic peak at 734 cm^{-1} was clearly visible when high concentrations of MRSA were present. When the concentration decreased to 10^6 CFU mL^{-1}, the characteristic peak at 734 cm^{-1} could still be distinguished from interfering peak, and MRSA could still be specifically recognised. The results show that the paper substrate of the $Ti_3C_2T_x$-AuNP is anti-interference for the detection of bacteria.

Compared with the method of direct SERS detection of bacteria without complex capture and labeling (Table S1†), the detection limits of paper substrate of $Ti_3C_2T_x$-AuNP for E. coli and MRSA reached 10^5 CFU mL^{-1} and 5×10^5 CFU mL^{-1} respectively. It shows good SERS ability to directly detect bacteria.

3.3. Evaluation of antibacterial activity

Infection of humans by microorganisms has the probability of causing many serious diseases. In addition to the ability to
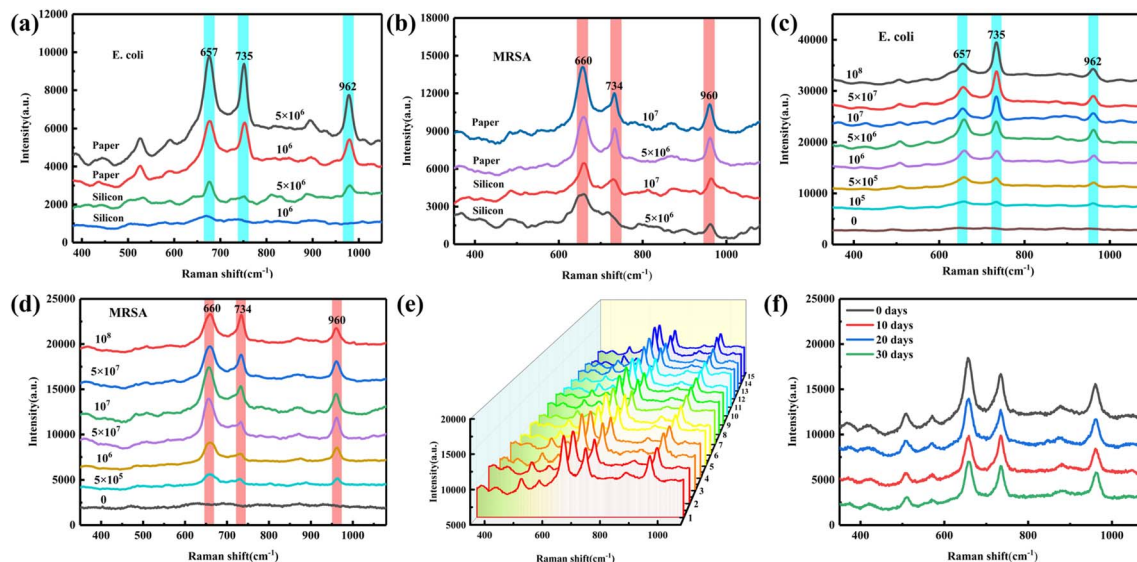
Fig. 3 (a) SERS spectral of *E. coli*: 5×10^6 and 10^6 CFU mL^{-1} on paper-based and silicon-based substrate. (b) SERS spectral of MRSA: 10^7 and 5×10^6 CFU mL^{-1} on paper-based and silicon-based substrate. (c) SERS spectral of *E. coli* under different concentrations: 0 CFU mL^{-1} to 10^8 CFU mL^{-1} (d) SERS spectral of MRSA under different concentrations: 0 CFU mL^{-1} to 10^8 CFU mL^{-1}. SERS spectra of *E. coli* (5×10^6 CFU mL^{-1}): on 15 arbitrary spots of the paper substrate of Ti$_3$C$_2$T$_x$-AuNP (e) and on the Ti$_3$C$_2$T$_x$-AuNP paper-based within 1 month (f).

detect bacteria, the prepared paper substrate of Ti$_3$C$_2$T$_x$-AuNP was also investigated as bactericidal materials. As stated above, the risk to human health from *E. coli* and MRSA should not be underestimated. After rapid detection of the bacteria, it is more important to continue to effectively kill the pathogenic bacteria. In order to evaluate the bactericidal ability of the materials, the Gram-negative bacterium *E. coli* and the Gram-positive bacterium MRSA were selected as typical strains, and the antibacterial effect of the paper substrate of Ti$_3$C$_2$T$_x$-AuNP was evaluated by the colony counting method. 5 µL of bacteria (10^{10} CFU mL^{-1}) suspension was dropped on cellulose paper soaked in 200–800 µg mL^{-1} Ti$_3$C$_2$T$_x$-AuNP, Ti$_3$C$_2$T$_x$ and AuNP, and incubated on the shaker (37 °C, 200 rpm) for 5 hours. In this experiment, the concentrations of Ti$_3$C$_2$T$_x$ and AuNP were the same as those in Ti$_3$C$_2$T$_x$-AuNP of 600 µg mL^{-1}.

Fig. S1† shows typical photographs of *E. coli* and MRSA colonies after treatment of cellulose paper with different concentrations of Ti$_3$C$_2$T$_x$-AuNP. The pictures show that as the concentration of Ti$_3$C$_2$T$_x$-AuNP increased, the number of colonies appeared to decrease. It means that paper substrate of Ti$_3$C$_2$T$_x$-AuNP showed some antibacterial activity against both Gram-negative and Gram-positive bacteria. As shown in Fig. 4a and b, the survival rates of *E. coli* and MRSA after treatment were counted. With the increase of Ti$_3$C$_2$T$_x$-AuNP concentration, the survival rate of bacteria both showed decrease. It is obvious that the bactericidal rate of the paper substrate of Ti$_3$C$_2$T$_x$-AuNP for bacteria shows a dependence on the concentration of the Ti$_3$C$_2$T$_x$-AuNP. After 5 h of co-cultivation, the survival rate of *E. coli* and MRSA at a Ti$_3$C$_2$T$_x$-AuNP concentration of 600 µg mL^{-1} decreased to 53.76% and 50%, respectively, proving that the paper substrate of Ti$_3$C$_2$T$_x$-AuNP has a certain degree of bacteriostatic ability. Meanwhile, cellulose paper impregnated by Ti$_3$C$_2$T$_x$ and AuNP also showed some degree of

sterilization. For *E. coli*, the survival rates of cellulose paper soaked with Ti$_3$C$_2$T$_x$ and AuNP were 60.12% and 70.01%, respectively.

For MRSA, the survival rates of cellulose paper soaked with Ti$_3$C$_2$T$_x$ and AuNP were 86.04% and 97.67%, respectively. It is easy to see that the sterilization rate of cellulose paper soaked with Ti$_3$C$_2$T$_x$ or AuNP alone is lower than that of Ti$_3$C$_2$T$_x$-AuNP with the respective content. In order to further explore the sterilization mechanism of the material, Fig. S2† showed the morphological changes of *E. coli* and MRSA before and after treatment, respectively. In the SEM images of cellulose paper soaked in NaCl solution (0.9%) (Fig. S2a and S2c†), both *E. coli* and MRSA had intact smooth surfaces. *E. coli* and MRSA bacterial cells were recultivated after treatment with cellulose paper soaked in 600 µg mL^{-1} Ti$_3$C$_2$T$_x$-AuNP nanocomposite, the bacteria were ruptured to varying degrees (Fig. S2b and S2d†). This maybe since the monolayer MXene has sharp edges. It was concluded that prepared paper substrate of Ti$_3$C$_2$T$_x$-AuNP was able to inhibit bacterial growth by contact killing.

3.4. Photothermal effect of paper substrate of Ti$_3$C$_2$T$_x$-AuNP

Obviously, the antibacterial power of Ti$_3$C$_2$T$_x$-AuNP alone does not achieve the desired bactericidal effect. In addition to bacteriostatic effect of Ti$_3$C$_2$T$_x$-AuNP itself through contact killing, Ti$_3$C$_2$T$_x$-AuNP can also achieve sterilization through photothermal therapy. It has been reported that bacteria are irreversibly damaged when the ambient temperature is maintained at 55 °C for period.[34,35] Near-infrared photothermal therapy (PTT) is known for its deep penetration suitable for biological applications, and its excellent photothermal conversion ability can realize effective killing of bacteria in a short period of time. Previous work in this paper has shown that both
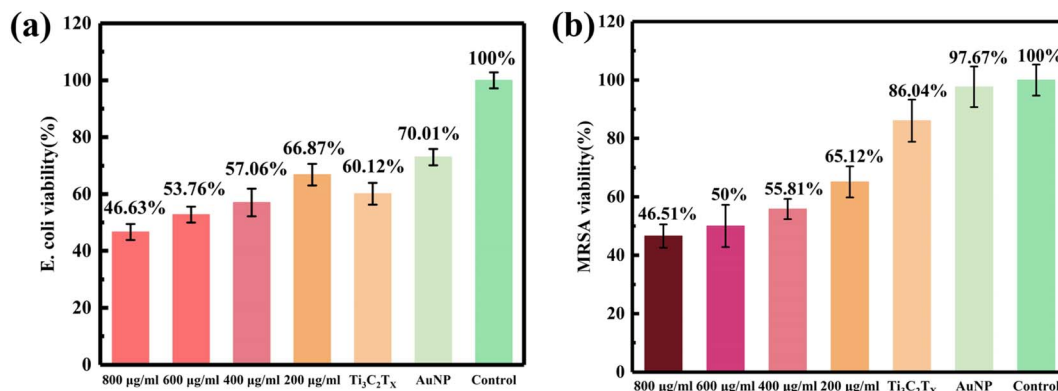
Fig. 4 Bacterial viability measurements of *E. coli* (a) and MRSA (b) grown on fresh LB agar plates for 24 h: recultivated after treatment with cellulose paper soaked in 200 μg mL^{-1} to 800 μg mL^{-1} Ti$_3$C$_2$T$_x$-AuNP nanocomposite, Ti$_3$C$_2$T$_x$, AuNP and NaCl solution (0.9%), respectively.

Ti$_3$C$_2$T$_x$ and Ti$_3$C$_2$T$_x$-AuNP exhibit unique absorptions at NIR-I (Fig. 2c), exhibiting localized surface plasmon resonance effects. The absorption is located within the biological NIR window resulting in high penetration depth and low body damage, which is favourable for biological applications.[9] For 808 nm laser, the laser power density below 300 mW cm^{-2} is considered harmless to the human body.[21] Therefore, the photothermal properties of the prepared materials were evaluated to explore the possibility of using paper substrate of Ti$_3$C$_2$T$_x$-AuNP for low-power photothermal antibacterial applications.

As shown in Fig. 5a, at the same concentration of Ti$_3$C$_2$T$_x$, paper substrate of Ti$_3$C$_2$T$_x$-AuNP has a higher absorbance at 808 nm than paper substrate of Ti$_3$C$_2$T$_x$. This may allow for a higher temperature rise for it in the same situation. Herein, a paper substrate in a dry state was irradiated with low laser power (300 mW cm^{-2}). The results showed that at low laser power it takes only a few seconds for the temperature of the cellulose paper to rise to an extremely high level (Fig. S3,† above 90 °C).

Fig. S4 and S5† illustrates the temperature increase of cellulose paper soaked with different concentrations of Ti$_3$C$_2$T$_x$-AuNP when irradiated with 300 mW cm^{-2} laser power, which showed the excellent ability of the paper substrate of Ti$_3$C$_2$T$_x$-AuNP for fast photothermal conversion at low laser power. In order to simulate the application of cellulose paper over wet wounds or *in vivo*, moist cellulose paper was used to simulate these scenarios. The moist cellulose paper soaked in 600 μg mL^{-1} Ti$_3$C$_2$T$_x$-AuNP nanocomposite was exposed to 808 nm laser with different laser power densities (100, 200, 300 and 400 mW cm^{-2}). As shown in Fig. 5b, the temperature of the cellulose paper increased rapidly within 5 seconds and remained near the maximum temperature. In addition, the temperature change of the solution is closely related to the laser power density. For example, the moist cellulose paper soaked in 600 μg mL^{-1} Ti$_3$C$_2$T$_x$-AuNP nanocomposite could reach 73.1 °C under 400 mW cm^{-2} laser irradiation, while a same moist cellulose paper reached 42.7 °C under 100 mW cm^{-2} laser irradiation. Fig. 5c shows the temperature trends of different materials under NIR radiation (300 mW cm^{-2} for 30 s). The temperature of H$_2$O

remained almost unchanged, and the temperature of Ti$_3$C$_2$T$_x$ cellulose paper increased to 41.2 °C. In the case of paper substrate of Ti$_3$C$_2$T$_x$, concentrations above 400 μg mL^{-1} can quickly reach temperature above 55 °C, which can effectively destroy the bacteria. The temperature of paper substrate of Ti$_3$C$_2$T$_x$-AuNP increases higher than that of pure Ti$_3$C$_2$T$_x$, which implies that paper substrate of Ti$_3$C$_2$T$_x$-AuNP has better photothermal properties. Meanwhile, the temperature rise of the paper substrate of Ti$_3$C$_2$T$_x$-AuNP is concentration-dependent. Thermal imaging showed that as the concentration increased, the temperature reached by the paper substrate also increased. These results are supported by the infrared thermography in Fig. 5d. In order to verify the photothermal stability of the paper substrate, the NIR photothermal conversion ability of the moist cellulose paper soaked in 600 μg mL^{-1} Ti$_3$C$_2$T$_x$-AuNP was examined under 808 nm continuous-wave laser irradiation (300 mW cm^{-2}) (Fig. 5e). No significant attenuation of the temperature increase was observed over five consecutive cycles of the laser switching process, which reveals the high photothermal stability of Ti$_3$C$_2$T$_x$-AuNP. The above experiments verified the photothermal performance of the paper substrate of Ti$_3$C$_2$T$_x$-AuNP in very short time at low laser power, indicating that paper substrate of Ti$_3$C$_2$T$_x$-AuNP has ability to convert 808 nm near-infrared light energy into thermal energy quickly and efficiently.

3.5. Photothermal antibacterial activity of paper substrate of Ti$_3$C$_2$T$_x$-AuNP

Since paper substrate of Ti$_3$C$_2$T$_x$-AuNP exhibit excellent photothermal properties, the above results suggest that paper substrate of Ti$_3$C$_2$T$_x$-AuNP offer the possibility of further application for photothermal sterilization. Similar to the previous work, paper substrate dripped with bacterial fluids were immediately illuminated with 808 nm laser (5 min, 300 mW cm^{-2}). After the irradiation is completed, the paper incubated on the shaker (37 °C, 200 rpm) for 5 hours. Finally, aliquots of the samples were withdrawn and CFU were counted as described previously. As shown in Fig. 6a, it can be clearly seen that after NIR irradiation, the number of bacteria on the LB
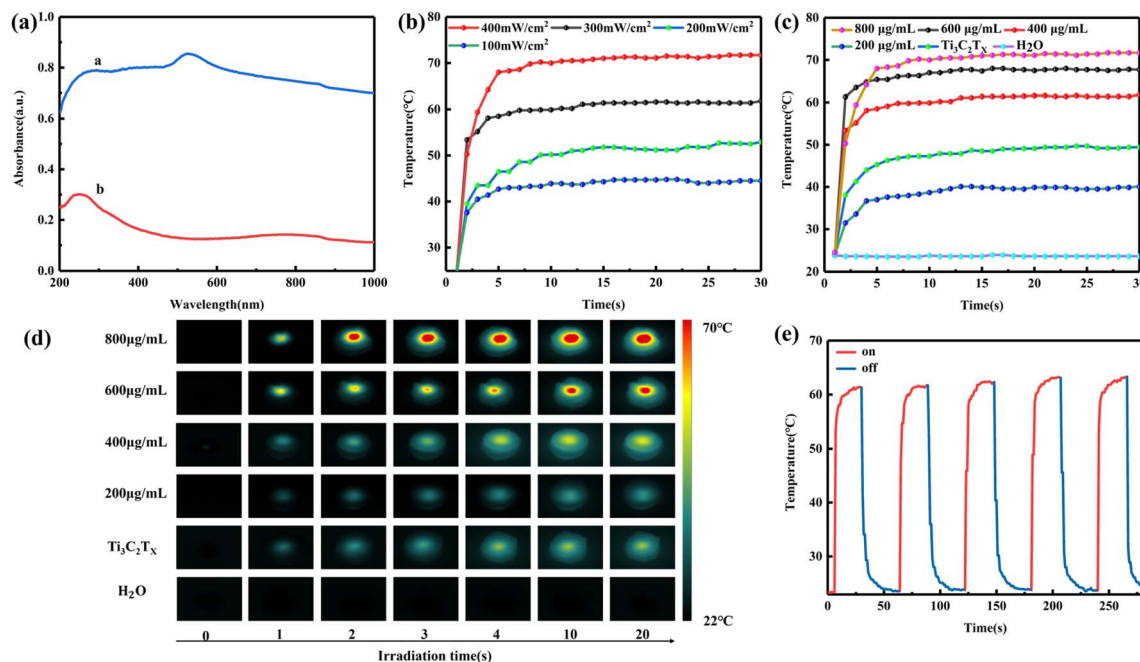
Fig. 5 (a) UV-vis spectra of paper substrate of Ti$_3$C$_2$T$_x$-AuNP and paper substrate of Ti$_3$C$_2$T$_x$. Photothermal effects of moist paper substrate of Ti$_3$C$_2$T$_x$-AuNP: (b) temperature changes of moist cellulose paper soaked in 600 µg mL^{-1} Ti$_3$C$_2$T$_x$-AuNP nanocomposite with a series of power densities of 808 nm laser irradiation. Temperature changes (c) and thermal imaging (d) after NIR irradiation (300 mW cm^{-2}) for 20 s with various materials and different concentrations of Ti$_3$C$_2$T$_x$-AuNP. (e) Photothermal heating curves of moist cellulose paper soaked in 600 µg mL^{-1} Ti$_3$C$_2$T$_x$-AuNP nanocomposite for five cycles under laser on/off cycles with 808 nm laser (300 mW cm^{-2}) irradiation.

agar plates of the samples after co-incubation with paper substrate of Ti$_3$C$_2$T$_x$-AuNP was significantly reduced compared to the bacteria treated with NaCl solution. Photothermal sterilization using pure Ti$_3$C$_2$T$_x$ and pure AuNP were performed as a control experiment. As shown in Fig. 6c and d, the number of bacteria on the LB agar plates was reduced after NIR irradiation. For pure Ti$_3$C$_2$T$_x$, the photothermal sterilization of *E. coli* and MRSA was 57.59% and 45.3%, respectively. And for pure AuNP, the photothermal sterilization of *E. coli* and MRSA was 65.06% and 88.4%, respectively. Compared with pure Ti$_3$C$_2$T$_x$ or AuNP, the photothermal sterilization rate of paper substrate of Ti$_3$C$_2$T$_x$-AuNP was significantly improved. It was estimated that photothermal sterilization of *E. coli* and MRSA could reach more than 99.94% and 92.71%, respectively, when the immersion concentration was higher than 600 µg mL^{-1}. The significant increase in photothermal sterilization rate as compared to the antibacterial experiment may be due to the synergistic effect of NIR radiation and paper substrate of Ti$_3$C$_2$T$_x$-AuNP. The bacterial morphology of *E. coli* and MRSA treated with NaCl solution was observed by SEM images (Fig. 6a–c), and both *E. coli* and MRSA remained intact and smooth, with hardly any damaged bacteria observed. However, after treatment with paper substrate of Ti$_3$C$_2$T$_x$-AuNP and NIR, the cell membranes were obviously ruptured, which indicated that the bacterial walls of the bacterial cells were severely damaged. Previous reports have shown that common bacteria such as *E. coli* are irreversibly and severely damaged at temperatures of 55 °C. In this work, paper substrate of Ti$_3$C$_2$T$_x$-AuNP can strongly absorb light energy and convert it into heat upon near-infrared laser

irradiation, which can damage the bacterial cell wall of bacteria by high-temperature ablation and lead to the death of bacteria. According to ANSI Z136.1–2014 (American National Standard for Safe Use of Lasers), the maximum permissible exposure (MPE) corresponding to 808 nm laser is 330 mW cm^{-2} (ref. 21 and 22). Compared with previous work (Table S2†) under the irradiation of 808 nm laser (300 mW cm^{-2}), the paper substrate of Ti$_3$C$_2$T$_x$-AuNP prepared in this paper could be heated to 67.2 °C in just 5 seconds, thus rapidly converting light energy into heat energy. The photothermal sterilization rates were 99.94% and 92.71% for *E. coli* and MRSA after only 5 minutes, respectively. Thus, our work provides a basis for the efficient sterilization strategies under safe laser power.

3.6. Capacity to generate reactive oxygen species

In order to counteract the resistance generated by the overuse of antibiotics, photodynamic therapy can be utilized in addition to photothermal therapy.[36,37] As has been reported, light can activate photosensitizing materials that kill pathogens by generating reactive oxygen species (ROS). The ROS produced during treatment can lead to apoptosis or necrosis of the pathogen by physically damaging its cell membrane. It has been reported that MXene can generate ROS, which is expected to enable the paper substrate of Ti$_3$C$_2$T$_x$-AuNP to further enhance bactericidal capabilities through photodynamic therapy. In this study, hydroxyl radical (•OH), superoxide anion radical (O2•$^-$) and singlet oxygen ^{1}O$_2$ were considered as possible ROS generated and were detected by their corresponding probes, respectively.
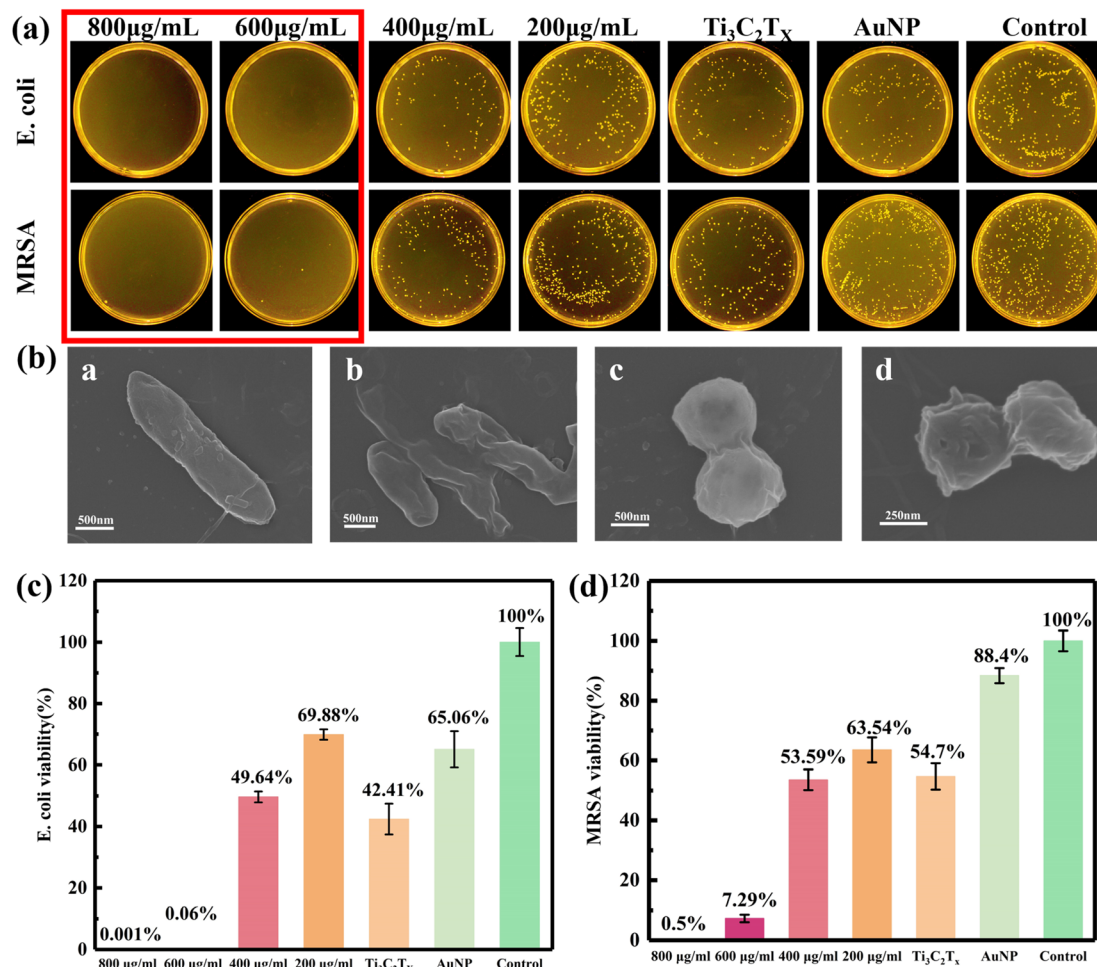
Fig. 6 (a) Antibacterial activities in aqueous suspensions with NIR irradiation (808 nm, 300 mW cm^{-2}, 5 min) after 5 h: bacterial suspensions with cellulose paper soaked in NaCl solution (0.9%) with NIR irradiated were used as control. Photographs of agar plates onto which *E. coli* and MRSA bacterial cells were recultivated after treatment with cellulose paper soaked in 200 μg mL^{-1} to 800 μg mL^{-1} Ti$_3$C$_2$T$_x$-AuNP nanocomposite, Ti$_3$C$_2$T$_x$ and AuNP, respectively. (b) SEM images of the *E. coli* (b) and MRSA (d) treated with cellulose paper soaked in 600 μg mL^{-1} of Ti$_3$C$_2$T$_x$-AuNP. Control bacterial cells (a and c). Bacterial viability measurements of *E. coli* (c) and MRSA (d) with NIR irradiated (808 nm, 300 mW cm^{-2}, 5 min) grown on fresh LB agar plates for 24 h: recultivated after treatment with cellulose paper soaked in 200 μg mL^{-1} to 800 μg mL^{-1} Ti$_3$C$_2$T$_x$-AuNP nanocomposite, Ti$_3$C$_2$T$_x$ (e), AuNP (f) and NaCl solution (0.9%), respectively.

To detect the generation of reactive oxygen species, 808 nm laser irradiation was applied to paper substrate of Ti$_3$C$_2$T$_x$-AuNP immersed in several probe solutions for 30 minutes. As control, the paper substrate of Ti$_3$C$_2$T$_x$-AuNP was immersed in the probe solutions but no laser irradiation. Under laser irradiation, the $^{\bullet}$OH generated on the surface of the paper substrate of Ti$_3$C$_2$T$_x$-AuNP oxidized the colourless OPD to produce diaminophenazine (DAP), which was yellow in colour and had a fluorescent signal. In contrast to before laser irradiation (Fig. 7a), the absorbance at 420 nm of the mixed solution after laser irradiation increased significantly with time (Fig. 7d). The O$_2^{\bullet-}$ generated from the paper substrate of Ti$_3$C$_2$T$_x$-AuNP under laser irradiation reacted with NBT to form a blue-violet formazan, which showed a decrease in absorbance at 260 nm. Compared with no laser irradiation (Fig. 7b), the absorbance at 260 nm of the laser-irradiated mixed solution decreased with increasing irradiation time (Fig. 7e). DPBF was chosen as a ROS

probe for the measurement of the amount of ^{1}O$_2$ produced under light conditions. DPBF is a commonly used singlet oxygen indicator that binds to singlet oxygen in solution and is also sensitive to trace amounts of ^{1}O$_2$. Therefore, the production of ^{1}O$_2$ by the sample can be known by measuring the change in the UV absorption peak of DPBF in a solution of paper substrate of Ti$_3$C$_2$T$_x$-Au mixed with DPBF. As shown in Fig. 7f, the absorbance of the solution at 418 nm decreased slightly after laser irradiation.

The above experimental results indicate that the paper substrate of Ti$_3$C$_2$T$_x$-AuNP produces a variety of reactive oxygen species under 808 nm laser irradiation, which has certain photodynamic properties. This is promising to help the paper substrate of Ti$_3$C$_2$T$_x$-AuNP combine the material itself antibacterial, photothermal therapy and photodynamic therapy, to achieve combined antibacterial and improved bactericidal efficacy. Therefore, the prepared paper substrate of Ti$_3$C$_2$T$_x$-Au is
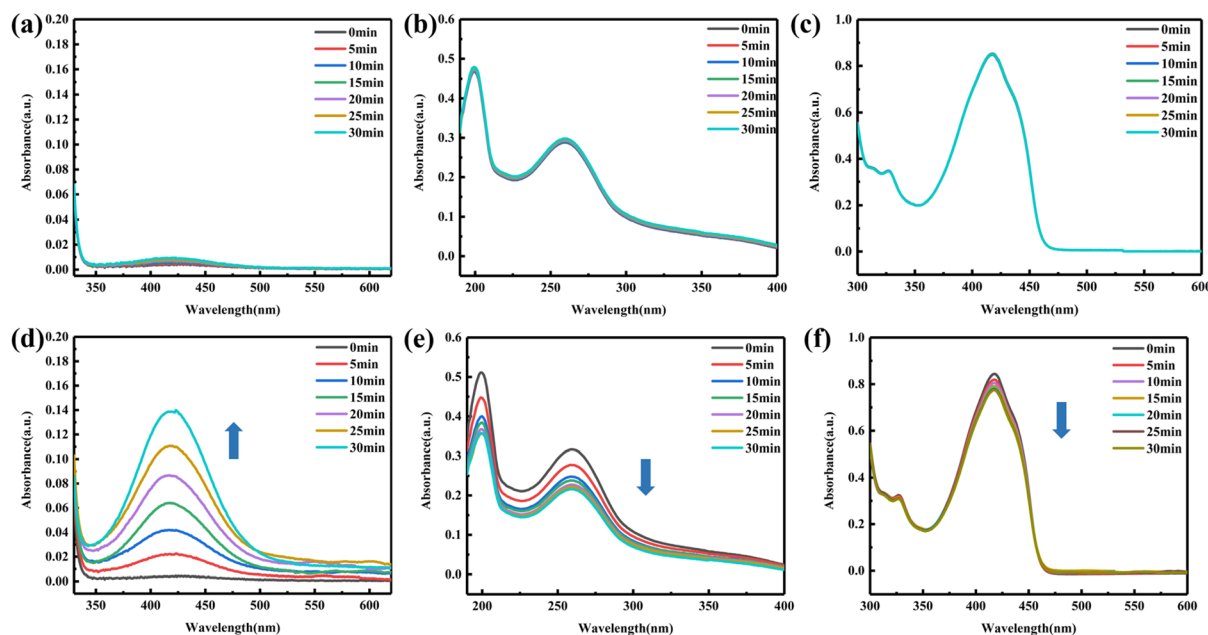
Fig. 7 UV–vis spectra of OPD (a), NBT (b), DPBF (c). UV–vis spectra of OPD (d), NBT (e), DPBF (f) with 808 nm irradiation (300 mW cm^{-2}, 30 min) on paper substrate of Ti$_3$C$_2$T$_x$-Au.

a material for simultaneous detection of bacteria and photothermal sterilization, which is expected to be a platform for simultaneous diagnosis and precise treatment of bacteria.

4. Conclusions

In summary, paper substrate of Ti$_3$C$_2$T$_x$-AuNP was successfully synthesized by a self-assembly and freeze-drying method, which uniformly attached Ti$_3$C$_2$T$_x$-AuNP to the surface of cellulose. The prepared flexible paper substrates can be used for non-contact sensitive SERS detection of bacteria without the need for tedious pretreatment, labelling and specific aptamers. In addition, compared to the common silicon-based SERS substrate, the flexible paper-based SERS substrate has the advantages of being more portable, fitting more closely to the surface to be inspected, and being able to be split for inspection. The paper substrate was used as a SERS substrate for bacterial detection with detection limits as low as 10^5 CFU mL^{-1} and 5 × 10^5 CFU mL^{-1} for *E. coli* and MRSA, respectively, demonstrating the paper substrate's ability to detect bacteria with sensitivity. The antibacterial properties of the materials were subsequently tested by colony counting method, which showed a concentration-dependent bacterial survival rate. The survival rates of cellulose paper soaked in 600 μg mL^{-1} Ti$_3$C$_2$T$_x$-AuNP nanocomposite against *E. coli* and MRSA were 53.76% and 50%, respectively, which proved that the material has certain antibacterial properties. Furthermore, under the irradiation of 808 nm laser (300 mW cm^{-2}), the temperature of paper substrate of Ti$_3$C$_2$T$_x$-AuNP could be increased to 67.2 °C in just 5 seconds, which rapidly converted the light energy into heat energy. The photothermal sterilization rates were 99.94% and 92.71% for *E. coli* and MRSA, respectively. The SEM images

of the bacteria showed that the photothermal sterilization caused irreversible damage to the bacterial cells and might lead to bacterial death. The multiple reactive oxygen species generated by paper substrate of Ti$_3$C$_2$T$_x$-AuNP are likely to provide further guarantee for stable sterilization. Therefore, the prepared novel multifunctional self-assembled paper substrate of Ti$_3$C$_2$T$_x$-AuNP can rapidly and sensitively label-free detect bacteria based on SERS and effectively inhibit bacterial, photothermal or photodynamic sterilization at low laser power. It is expected to be applied in the fields of antibacterial of human wounds under safe laser and resistance to drug-resistant bacteria.

Conflicts of interest

There are no conflicts to declare.

Acknowledgements

References

1 J. Davies and D. Davies, *Microbiol. Mol. Biol. Rev.*, 2010, **74**, 417–433.
2 M. R. Gillings, *Microbiol. Mol. Biol. Rev.*, 2014, **78**, 257–277.
3 Q. Y. Zhang, Z. B. Yan, Y. M. Meng, X. Y. Hong, G. Shao, J. J. Ma, X. R. Cheng, J. Liu, J. Kang and C. Y. Fu, *Mil. Med. Res.*, 2021, **8**, 25.

4 A. Abbaspour, F. Norouz-Sarvestani, A. Noon and N. Soltani, *Biosens. Bioelectron.*, 2015, **68**, 149–155.

5 N. M. Danesh, M. Ramezani, A. S. Emrani, K. Abnous and S. M. Taghdisi, *Biosens. Bioelectron.*, 2016, **75**, 123–128.

6 C. Y. Zhang, L. J. Huang, H. B. Pu and D. W. Sun, *Trends Food Sci. Technol.*, 2021, **113**, 366–381.

7 G. Q. Fang, X. Lin, X. Liang, J. L. Wu, W. Xu, W. L. J. Hasi and B. Dong, *Small*, 2022, **18**, 12.

8 D. Wang, G. C. Xu, X. S. Zhang, H. Y. Gong, L. Jiang, G. L. Sun, Y. Li, G. R. Liu, Y. Li, S. K. Yang and X. Liang, *Sens. Actuators, B*, 2022, **359**(11), 131512.

9 A. Sarycheva, T. Makaryan, K. Maleski, E. Satheeshkumar, A. Melikyan, H. Minassian, M. Yoshimura and Y. Gogotsi, *J. Phys. Chem. C*, 2017, **121**, 19983–19988.

10 A. Sinha, Dhanjai, H. Zhao, Y. Huang, X. Lu, J. Chen and R. Jain, *TrAC, Trends Anal. Chem.*, 2018, **105**, 424–435.

11 R. Y. Liu, L. Jiang, C. X. Lu, Z. Z. Yu, F. H. Li, X. F. Jing, R. Xu, W. Zhou and S. Z. Jin, *Spectrochim. Acta, Part A*, 2020, **236**, 8.

12 Z. Z. Yu, L. Jiang, R. Y. Liu, W. D. Zhao, Z. H. Yang, J. Y. Zhang and S. Z. Jin, *Chem. Eng. J.*, 2021, **426**, 12.

13 R. Y. Liu, L. Jiang, Z. Z. Yu, Y. Chen, R. Xu and S. Z. Jin, *Appl. Opt.*, 2020, **59**, 7846–7852.

14 K. C. Xu, R. Zhou, K. Takei and M. H. Hong, *Adv. Sci.*, 2019, **6**, 23.

15 A. A. Shamsabadi, M. S. Gh, B. Anasori and M. Soroush, *ACS Sustain. Chem. Eng.*, 2018, **6**, 16586–16596.

16 Y. W. Zheng, Y. L. Yan, L. M. Lin, Q. He, H. H. Hu, R. Luo, D. Y. Xian, J. Y. Wu, Y. Shi, F. P. Zeng, C. B. Wu, G. L. Quan and C. Lu, *Acta Biomater.*, 2022, **142**, 113–123.

17 C. H. Yu, S. Y. Sui, X. T. Yu, W. L. Huang, Y. F. Wu, X. Zeng, Q. M. Chen, J. Wang and Q. Peng, *Colloids Surf., B*, 2022, **217**, 8.

18 Y. J. Gao, Y. H. Dong, S. T. Yang, A. C. Mo, X. Zeng, Q. M. Chen and Q. Peng, *J. Colloid Interface Sci.*, 2022, **617**, 533–541.

19 L. Ma, X. B. Feng, H. Liang, K. Wang, Y. Song, L. Tan, B. J. Wang, R. J. Luo, Z. W. Liao, G. C. Li, X. M. Liu, S. L. Wu and C. Yang, *Mater. Today*, 2020, **36**, 48–62.

20 J. T. Robinson, S. M. Tabakman, Y. Y. Liang, H. L. Wang, H. S. Casalongue, D. Vinh and H. J. Dai, *J. Am. Chem. Soc.*, 2011, **133**, 6825–6831.

21 R. Zhu, F. Gao, J. G. Piao and L. H. Yang, *Biomater. Sci.*, 2017, **5**, 1596–1602.

22 Q. S. Wang, H. Wang, Y. Yang, L. H. Jin, Y. Liu, Y. Wang, X. Y. Yan, J. Xu, R. Q. Gao, P. P. Lei, J. J. Zhu, Y. H. Wang, S. Y. Song and H. J. Zhang, *Adv. Mater.*, 2019, **31**, 7.

23 G. Y. Liu, J. H. Zou, Q. Y. Tang, X. Y. Yang, Y. W. Zhang, Q. Zhang, W. Huang, P. Chen, J. J. Shao and X. C. Dong, *ACS Appl. Mater. Interfaces*, 2017, **9**, 40077–40086.

24 J. Luo, X. Tao, J. Zhang, Y. Xia, H. Huang, L. Zhang, Y. Gan, C. Liang and W. Zhang, *ACS Nano*, 2016, **10**, 2491–2499.

25 A. Sarycheva and Y. Gogotsi, *Chem. Mater.*, 2020, **32**, 3480–3488.

26 G. Frens, *Nature Phys. Sci.*, 1973, **241**, 20–22.

27 H. Huang, C. H. Dong, W. Feng, Y. Wang, B. C. Huang and Y. Chen, *Adv. Drug Delivery Rev.*, 2022, **184**, 40.

28 X. X. Xue, L. Chen, C. M. Zhao, M. Lu, Y. Qiao, J. Wang, J. H. Shi and L. M. Chang, *Spectrochim. Acta, Part A*, 2023, **302**, 7.

29 M. Bonnet, E. Buc, P. Sauvanet, C. Darcha, D. Dubois, B. Pereira, P. Dechelotte, R. Bonnet, D. Pezet and A. Darfeuille-Michaud, *Clin. Cancer Res.*, 2014, **20**, 859–867.

30 S. Lakhundi and K. Y. Zhang, *Clin. Microbiol. Rev.*, 2018, **31**, 103.

31 S. Ramos, V. Silva, M. D. E. Dapkevicius, M. Caniça, M. T. Tejedor-Junco, G. Igrejas and P. Poeta, *Animals*, 2020, **10**, 15.

32 S. Bashir, H. Nawaz, M. I. Majeed, M. Mohsin, S. Abdullah, S. Ali, N. Rashid, M. Kashif, F. Batool, M. Abubakar, S. Ahmad and A. Abdulraheem, *Photodiagn. Photodyn. Ther.*, 2021, **34**, 12.

33 X. P. Chen, M. Q. Tang, Y. Liu, J. Q. Huang, Z. Y. Liu, H. Y. Tian, Y. T. Zheng, M. L. de la Chapelle, Y. Zhang and W. L. Fu, *Microchim. Acta*, 2019, **186**, 8.

34 C. Mutalik, I. H. Lin, D. I. Krisnawati, S. Khaerunnisa, M. Khafid, Widodo, Y. C. Hsiao and T. R. Kuo, *Int. J. Nanomed.*, 2022, **17**, 6821–6842.

35 S. Yougbare, H. L. Chou, C. H. Yang, D. I. Krisnawati, A. Jazidie, M. Nuh and T. R. Kuo, *J. Hazard. Mater.*, 2021, **407**, 8.

36 T. Dutta, R. Sarkar, B. Pakhira, S. Ghosh, R. Sarkar, A. Barui and S. Sarkar, *RSC Adv.*, 2015, **5**, 80192–80195.

37 H. T. Yuan, X. P. Hong, H. Ma, C. J. Fu, Y. D. Guan, W. Huang, J. B. Ma, P. Xia, M. Cao, L. H. Zheng, X. L. Xu, C. C. Xu, D. Z. Liu, Z. J. Li, Q. S. Geng and J. G. Wang, *ACS Mater. Lett.*, 2023, 762–774.